TECHNICAL MEMORANDUM
X-135

TRANSONIC FLUTTER CHARACTERISTICS OF A 45° SWEPTBACK WING WITH VARIOUS DISTRIBUTIONS OF BALLAST ALONG THE LEADING EDGE

By John R. Unangst

Langley Research Center
Langley Field, Va.

NATIONAL AERONAUTICS AND SPACE ADMINISTRATION
WASHINGTON

December 1959
Declassified January 12, 1961

NATIONAL AERONAUTICS AND SPACE ADMINISTRATION

TECHNICAL MEMORANDUM X-135

TRANSONIC FLUTTER CHARACTERISTICS OF A 45° SWEPTBACK WING WITH VARIOUS DISTRIBUTIONS OF BALLAST ALONG THE LEADING EDGE*

By John R. Unangst

SUMMARY

An investigation of the use of ballast at the leading edge of a sweptback wing as a flutter fix has been made. The investigation was conducted in the Langley transonic blowdown tunnel with wing models which had an aspect ratio of 4, sweepback of the quarter-chord line of 45°, and a taper ratio of 0.2. Four ballast configurations, which included different amounts of ballast distributed at two different spanwise locations, were investigated. Full-span sting-mounted models were employed. Data were obtained over a Mach number range from 0.65 to 1.32.

Comparison of the data for the ballasted wings with data for a similar wing without ballast shows that in the often critical Mach number range between 0.85 and 1.05, the dynamic pressure required for flutter is increased by as much as 100 percent due to the addition of about 6 percent of the wing mass as ballast at the leading edge of the outboard sections. Furthermore, there are indications that similar benefits of leading-edge ballast can be obtained at Mach numbers above $M = 1.1$. Changing the spanwise location of the ballast and increasing the amount of the ballast by a factor of about 2 had very little additional effect on the dynamic pressure required for flutter. The possibility, therefore, exists that the beneficial effects obtained may be accomplished by using less than the minimum of about 6 percent of the wing mass as ballast as investigated in this paper.

INTRODUCTION

The results of a transonic flutter investigation of aspect-ratio-4, 45° sweptback wings with various center-of-gravity locations, reported

*Title, Unclassified.

in reference 1, showed that in the often critical transonic Mach number range the increase in dynamic pressure required for flutter resulting from a forward shift of the center-of-gravity location is considerably larger than that predicted by Theodorsen and Garrick in reference 2 for incompressible flow. The results of reference 1 therefore suggest the possibility of employing a forward shift of the center of gravity as a flutter fix at transonic Mach numbers. In reference 1 the center of gravity was moved forward by adding ballast to the wing leading edge along the entire wing span. A similar application of ballast to a full-scale airplane would probably be impractical because of the weight penalty involved. It should be noted, however, that shifting the center of gravity of the inboard sections forward may not be necessary to produce the desired increase in flutter speed because of the relatively low level of motion of the inboard sections in most flutter modes. The purpose of the present investigation is, therefore, to determine the effects of a forward shift of center of gravity of the outboard sections only.

The plan form selected for the present investigation had an aspect ratio of 4, sweepback of the quarter-chord line of 45°, and a taper ratio of 0.2. The data for the basic wing of this plan form are presented in reference 3. Models for the present investigation had the center of gravity of the outboard sections moved forward by the addition of ballast along the leading edge. Four ballast configurations were investigated over a Mach number range from 0.65 to 1.32. The flutter tests were conducted in the Langley transonic blowdown tunnel.

SYMBOLS

a	distance perpendicular to quarter-chord line, in wing semichords, from midchord to elastic axis, positive for elastic axis behind midchord
b	local wing semichord, perpendicular to quarter-chord line, ft
b_r	root semichord perpendicular to quarter-chord line at intersection of quarter-chord line and wing root, ft
b_s	streamwise root semichord, ft
b_t	streamwise tip semichord, ft
c	local wing chord, perpendicular to quarter-chord line, ft
f_e	experimental flutter frequency, cps

$f_{h,i}$ measured coupled bending frequency, cps (i = 1, 2, 3)

f_t measured first coupled torsion frequency, cps

l' exposed panel semispan perpendicular to model center line, ft

I_α mass moment of inertia per unit length of wing along quarter-chord line, measured about elastic axis, slug-ft^2/ft

M_e experimental Mach number

m mass of wing per unit length along quarter-chord line, slugs/ft

$\bar{m}$ total mass of exposed wing panel, slugs

q_e experimental dynamic pressure, lb/sq in.

r_α nondimensional radius of gyration about elastic axis, measured perpendicular to quarter-chord line, $\left(I_\alpha/mb^2\right)^{1/2}$

V_e experimental stream velocity, ft/sec

v volume of air within a conical frustrum having lower base diameter equal to streamwise root chord and upper base diameter equal to streamwise tip chord, $\frac{1}{3} l'\pi\left(b_s^2 + b_s b_t + b_t^2\right)$, cu ft

x_α distance in wing semichords from elastic axis to center of gravity, measured perpendicular to quarter-chord line; positive for center of gravity behind elastic axis

$x_{c.g.}$ distance perpendicular to quarter-chord line from leading edge to center of gravity, ft

η nondimensional coordinate along quarter-chord line measured from intersection of quarter-chord line and fuselage, fraction of quarter-chord-line length

$\bar{\mu}_e$ experimental mass ratio evaluated for entire exposed wing panel, $\bar{m}/\rho_e v$

ρ_e experimental air density, slugs/cu ft

ω_t measured first coupled circular torsion frequency, $2\pi f_t$, radians/sec

MODELS

Configurations

The plan form investigated had an aspect ratio of 4, sweepback of the quarter-chord line of 45°, and a taper ratio of 0.2 based on the chord in the model plane of symmetry. A total of nine models, all having NACA 65A003 streamwise airfoil sections, were employed. These models formed a series of four ballasted-wing configurations, the pertinent characteristics of which are tabulated below:

Configuration	Added ballast, percent of basic-wing panel mass	Spanwise extent of ballast, η
I	6.25	0.75 to 1.00
II	6.5	.50 to .75
III	10.9	.75 to 1.00
IV	12.5	.50 to .75

Model dimensions are shown in figure 1(a). Drawings of the models showing the location of the ballast for each configuration are presented in figures 1(b) and 1(c). A tabulation of the geometric properties of the models is presented in table I.

Construction

Each model was machined from a solid block of Consoweld, a phenolic laminate material with high-strength paper reinforcement (ref. 4). Prior to machining, each model block was inlaid with the ballast material (50 percent lead, 25 percent bismuth, and 25 percent tin, by weight) at the proper spanwise location (fig. 1). The Consoweld block plus the attached ballast was machined as a unit. The ballast was slotted normal to the quarter-chord line to minimize the effect of the ballast material on the overall stiffness of the wing panels (exposed semispans). Each surface of the wing panels was undercut by about 0.002 inch and then the panels were wrapped with 2 layers of 0.001-inch-thick Fiberglas (except model 7, which was wrapped with 2 layers of silk) to hold the ballast in place during the flutter tests. The 0.38-inch-thick center block of each model (fig. 1) was made flat and rectangular in shape to facilitate clamping the models in the sting support used in the wind-tunnel tests.

Physical Properties

Tabulations of the physical properties for each of the four ballast configurations are presented in tables II(a) to II(d). The properties, other than the natural frequencies, presented for single panels of models 1, 4, 7, and 9 are considered to be representative of all the models of configurations I, II, III, and IV, respectively. Spanwise distributions of mass per unit length of semispan, center-of-gravity location, and mass moment of inertia per unit length of semispan for the representative panels of the ballast configurations and for the basic wing are plotted in figure 2.

For the determination of the elastic-axis location a, each wing panel was clamped along a line perpendicular to the quarter-chord line and passing through the intersection of the wing trailing edge and the root. The chordwise position at which a concentrated bending load produced no twist in the wing was determined at several spanwise stations and a straight line faired through these points was taken to be the elastic-axis location. The parameters which define the spanwise distribution of mass, mass moment of inertia, and the center-of-gravity location (m, r_α^2, and x_α, respectively) were determined from strips cut perpendicular to the quarter-chord line for each panel. The total panel mass $\bar{m}$ was determined by weighing each panel prior to sawing it into strips. Each amount of added ballast indicated previously in the section entitled "Configurations" was determined by obtaining the area (shaded in fig. 2) between the curve for the mass distribution over the ballasted region and a curve which represented the estimated mass distribution of the particular wing without ballast.

The natural frequencies for all wing panels tested are tabulated in tables II(a) to II(d). The associated node lines are shown in figure 1. For the determination of the natural frequencies and node lines, each model was clamped to a steel bench in such a manner that each wing panel could be considered as cantilevered from the center block. An electromagnetic shaker was used to excite the models. Salt crystals sprinkled on the wing surface were used to identify the node lines.

APPARATUS AND TESTS

Wind Tunnel

The flutter tests were conducted in the Langley transonic blowdown tunnel. This tunnel is equipped with a slotted octagonal test section, measuring approximately 16 inches between flats, which allows Mach numbers from subsonic values to a maximum of about 1.4 to be obtained. During operation of the tunnel, a preselected Mach number is set by

means of a variable orifice downstream of the test section. This Mach number is held approximately constant, after the orifice is choked, while the stagnation pressure, and thus the density, is increased. The maximum stagnation pressure available is about 5 atmospheres. The static-density range is approximately 0.001 to 0.012 slug per cubic foot. It should be noted that because of the expansion of the air in the reservoir during a run, the stagnation temperature continually decreases so that the test-section velocity is not uniquely defined by the Mach number. The tunnel operating characteristics in terms of dynamic pressure q_e and Mach number M_e are indicated in figure 3 for four different orifice settings.

Support System

The models were supported in the tunnel by a 3-inch-diameter sting fuselage. The nose of the sting extended into the entrance cone of the test section, where the flow is always subsonic, to prevent the formation of a bow shock wave which might reflect from the tunnel walls onto the model. The complete support system weighed about 290 pounds and was considered to form a rigid mount for the models, since the mass of the system was very large compared with the mass of a model. The fundamental frequency of the support system was approximately 15 cycles per second.

Instrumentation

Electrical strain gages were mounted on the surface of each wing panel near the root. These gages were used to pick up the bending and torsional deflections of the wings and were so oriented that cross coupling between the bending and torsional deflections was minimized. A multichannel recording oscillograph was employed to record the time history of the strain-gage signals, tunnel-stagnation pressure and temperature, and test-section static pressure during the tests. Two cathode-ray oscilloscopes were employed in connection with the strain gages to aid the observer in detecting the occurrence of flutter during the tests. The strain-gage signals were fed to the oscilloscopes in such a way that a Lissajous figure appeared at flutter.

Tests

The objectives of the wind-tunnel tests were to determine the vibration frequency and the airspeed and density at flutter over a range of transonic Mach numbers. Flutter is obtained in the blowdown tunnel by gradually increasing the stagnation pressure until flutter is definitely identified by the observer, either by visual observation of the model or with the aid of the aforementioned oscilloscopes. Once flutter is obtained,

the stagnation pressure is held constant momentarily and then is quickly reduced. As was the case with the models of reference 3, the models of the present investigation had flutter boundaries so located within the operating range of the tunnel that data above $M = 1.05$ could not be obtained without flutter first being encountered between $M_e = 0.8$ and $M_e = 1.05$. Thus, attempts to obtain flutter at supersonic Mach numbers resulted in a start and stop of flutter between $M_e = 0.8$ and $M_e = 1.05$.

PRESENTATION OF DATA

The results of this investigation are tabulated in tables III(a) to III(d) for ballast configurations I to IV. In table III, the first column gives the identification numbers of the models employed in obtaining the data. The second column gives the run number and the third column shows the chronology of the data points obtained during a particular run. The fourth and fifth columns contain a code system which describes each data point. This code system is defined at the bottom of table III(a). (By way of explanation, low-damping behavior, indicated by the code letter D in table III, is characterized by a period of intermittent sinusoidal oscillations which obscures the exact start of flutter.) The column labeled f_t gives the torsion frequency (measured in still air) for the wing panel associated with the data point. Separate data points are presented for each panel throughout table III.

Data from table III are plotted as a function of Mach number in figures 4 to 7; these data are compared with data from reference 3 for the 3-percent-thick wing, referred to hereinafter as the basic wing. Data indicating the start of flutter are shown by open symbols; data indicating the end of flutter as the dynamic pressure was increasing are shown by flagged symbols; data indicating a no-flutter condition at the maximum dynamic pressure attained during a run are shown by solid symbols. Periods of low damping are indicated by dashed lines preceding the flutter points.

Figure 4 presents the variation of the parameter $\frac{V_e}{b_s \omega_t \sqrt{\bar{\mu}_e}}$ with Mach number for the four ballast configurations. Figures 5(a) to 5(d) present the variation with Mach number of the dynamic pressure required for flutter for ballast configurations I to IV, respectively. Figure 6 is a composite plot of the data in figures 5(a) to 5(d). Flutter frequency data for the four ballast configurations are presented in figure 7 in the form of the ratio of experimental flutter frequency to measured coupled torsion frequency plotted against Mach number.

DISCUSSION OF RESULTS

The data presented in figure 4 show that on the basis of the nondimensional parameter $\frac{V_e}{b_{s(n_t}\sqrt{\bar{\mu}_e}}$, the experimental results of the investigation tend to correlate for all ballast configurations. Figure 4 also shows substantially higher values of $\frac{V_e}{b_{s(n_t}\sqrt{\bar{\mu}_e}}$ for all ballasted wings than for the basic wing throughout the Mach number range of the investigation. This nondimensional presentation does not, however, make readily apparent the effect of the added ballast on the flutter speed and density of the basic wing, since the addition of ballast reduces the torsion frequency which is contained in the parameter. For a given wing the effectiveness of a flutter fix is illustrated more explicitly by comparing the results on the basis of dynamic pressure, as is done in figures 5 and 6.

Figure 5 shows that substantial increases in dynamic pressure required for flutter are realized throughout the Mach number range of the tests by adding a relatively small amount of ballast to the leading edge of the outboard sections of the basic wing. For example, figure 5(a) shows that the addition of about 6 percent of the basic wing mass as ballast increases the dynamic pressure required for flutter by as much as 100 percent in the often critical Mach number range between about $M_e = 0.85$ and $M_e = 1.05$. Since the dynamic pressure required for flutter varies directly with the torsional stiffness (to a first approximation), it thus appears that, in order to achieve the same effect produced by the addition of about 6 percent of the wing mass as ballast, an increase in plain-wing torsional stiffness by a factor of 2 would be required. A quantitative estimate of the effects of ballast at higher Mach numbers cannot be made, since flutter could not be obtained for this configuration above $M_e = 1.05$. However, the values of dynamic pressure associated with the no-flutter points in figure 5(a) do indicate that the flutter characteristics of this plan form above $M_e = 1.05$ can be substantially improved by the use of leading-edge ballast.

Figures 5(b) to 5(d) show that the results obtained for ballast configurations II, III, and IV are essentially the same as the results obtained for configuration I. It will be noted that there is some scatter in the data presented in figure 5, particularly for configuration IV (fig. 5(d)). However, the differences in natural frequencies between the two panels of some models and between some models of a given ballast configuration (table II) indicate that some scatter is to be expected.

The data presented in figure 5 are summarized and compared with the basic wing data in figure 6. In the Mach number range between $M_e = 0.65$

and $M_e = 0.95$ the data indicate that changing the spanwise location of the ballast and increasing the amount of ballast by about a factor of 2 had very little additional effect on the dynamic pressure required for flutter. The possibility, therefore, exists that the beneficial effects of leading-edge ballast indicated herein may be obtained by employing less than the minimum of 6.25 percent of the wing mass as ballast investigated herein. In the region near $M_e = 1.0$ the data in figure 6 show a considerable spread in dynamic pressure required for flutter. However, the location of the no-flutter points at supersonic Mach numbers indicates that near $M_e = 1.0$ the dynamic pressure required for flutter is changing very rapidly with Mach number. Hence, the data near $M_e = 1.0$ is believed to be indicating the trend of the flutter boundary in this region.

As shown in figure 7, the variation of the ratio of flutter frequency to torsion frequency with Mach number for the ballasted wings was essentially the same as that for the basic wing for Mach numbers up to 1.05.

It is recognized that some differences existed among the various models employed in the investigation. The differences in natural frequencies have been mentioned previously. From figure 2 it may be noted that, if the added ballast is disregarded, small differences exist in panel mass distribution for the various models. Furthermore, although no measurements were made, there were probably some slight differences in stiffnesses of the various models. However, these differences are believed to be small enough to have no appreciable effect on the conclusions of the present investigation.

CONCLUSIONS

The results of a transonic flutter investigation of an aspect-ratio-4, 45° sweptback, taper-ratio-0.2 plan form having various amounts and locations of leading-edge ballast indicate the following conclusions:

1. Substantial increases in dynamic pressure required for flutter were obtained throughout the Mach number range of the tests as a result of the addition of leading-edge ballast to the outboard sections of the basic wing. In the often critical Mach number range between Mach numbers of about 0.85 and about 1.05, the addition of as little as 6.25 percent of the basic wing mass as ballast increased the dynamic pressure at flutter by as much as 100 percent over that for the basic wing. Indications are that similar benefits of leading-edge ballast can be obtained at Mach numbers above $M = 1.1$.

2. Changing the spanwise location of the ballast and increasing the amount of ballast by a factor of about 2 had very little additional effect on the dynamic pressure required for flutter. The possibility therefore exists that the beneficial effects obtained may be accomplished by employing less than the minimum amount of ballast used in this investigation (6.25 percent of the wing mass).

Langley Research Center,
National Aeronautics and Space Administration,
Langley Field, Va., August 5, 1959.

REFERENCES

1. Jones, George W., Jr., and Unangst, John R.: Investigation to Determine Effects of Center-of-Gravity Location on the Transonic Flutter Characteristics of a 45° Sweptback Wing. NACA RM L55K30, 1956.

2. Theodorsen, Theodore, and Garrick, I. E.: Mechanism of Flutter - A Theoretical and Experimental Investigation of the Flutter Problem. NACA Rep. 685, 1940.

3. Unangst, John R.: Transonic Flutter Characteristics of an Aspect-Ratio-4, 45° Sweptback, Taper-Ratio-0.2 Plan Form. NASA TM X-136, 1959.

4. Lamb, J. J., Boswell, Isabelle, and Axilrod, B. M.: Tensile and Compressive Properties of Laminated Plastics at High and Low Temperatures. NACA TN 1550, 1948.

TABLE I.- GEOMETRIC PROPERTIES OF MODELS

NACA streamwise airfoil section	65A003
Aspect ratio (including body intercept)	4
Sweepback angle of quarter-chord line, deg	45
Taper ratio (based on chord in plane of symmetry)	0.2
Model span, ft	1.142
Exposed-wing-panel aspect ratio	1.83
Exposed-wing-panel taper ratio	0.241
Exposed-wing-panel semispan (perpendicular to model center line), l', ft	0.446
Length of exposed panel along quarter-chord line, ft	0.630
Root semichord perpendicular to quarter-chord line at intersection of quarter-chord line and exposed wing root, b_r, ft	0.1725
Streamwise root semichord, b_s, ft	0.1979

TABLE II.- PHYSICAL PROPERTIES OF MODELS

(a) Configuration I

Model 1 right panel $\bar{m}$ = 0.00186 slug

η	m, slugs/ft	r_α^2	a	x_α	b/b_r
0.379	0.00417	0.219	-0.178	0.086	0.7123
.463	.00348	.217	-.156	.042	.6486
.546	.00288	.231	-.134	.020	.5856
.626	.00233	.234	-.102	-.018	.5249
.710	.00183	.246	-.062	-.048	.4611
.792	.00221	.411	-.026	-.336	.3989
.875	.00177	.450	.036	-.424	.3359
.947	.00140	.561	.110	-.504	.2812

Measured natural frequencies

Item	Model 1		Model 2		Model 3	
	Left	Right	Left	Right	Left	Right
f_{h_1}	78.2	74.2	79.4	77.0	75.5	74.3
f_{h_2}	257	265	260	258	273	275
f_{h_3}	578	578	570	565	604	603
f_t	432	424	427	431	431	431
f_{h_1}/f_t	.181	.175	.186	.179	.175	.172
f_{h_2}/f_t	.595	.625	.609	.599	.633	.638
f_{h_3}/f_t	1.34	1.36	1.33	1.31	1.40	1.40

(b) Configuration II

Model 4 left panel $\bar{m}$ = 0.00191 slug

η	m, slugs/ft	r_α^2	a	x_α	b/b_r
0.369	0.00434	0.220	-0.074	-0.028	0.7199
.452	.00372	.235	-.052	-.056	.6559
.535	.00375	.332	-.018	-.222	.5939
.618	.00324	.332	.028	-.302	.5309
.701	.00281	.402	.078	-.414	.4679
.786	.00154	.312	.144	-.234	.4034
.868	.00113	.364	.240	-.318	.3412
.942	.000845	.479	.364	-.406	.2850

Measured natural frequencies

Item	Model 4	
	Left	Right
f_{h_1}	76.7	80
f_{h_2}	242	277
f_{h_3}	575	632
f_t	457	474
f_{h_1}/f_t	.168	.169
f_{h_2}/f_t	.530	.584
f_{h_3}/f_t	1.26	1.33

TABLE II.- PHYSICAL PROPERTIES OF MODELS - Concluded

(c) Configuration III

Model 7 right panel $\bar{m}$ = 0.00197 slug

η	m, slugs/ft	r_a^2	a	x_a	b/b_r
0.376	0.00125	0.234	-0.168	0.046	0.716
.460	.00358	.231	-.156	.048	.[illegible]
.544	.00293	.242	-.144	.036	.[illegible]
.625	.00236	.244	-.122	.022	.[illegible]
.710	.00189	.249	-.108	.032	.[illegible]
.792	.00287	.394	-.082	-.314	.[illegible]
.876	.00227	.351	-.028	-.382	.[illegible]
.945	.00180	.439	0.00	-.384	.[illegible]

Measured natural frequencies

Item	Model 5		Model 6		Model 7	
	Left	Right	Left	Right	Left	Right
f_{h_1}	58.2	57.3	59.7	66	63.5	66.2
f_{h_2}	238	237	253	271	228	248
f_{h_3}	531	540	577	612	553	585
f_t	420	431	448	438	410	427
f_{h_1}/f_t	.139	.133	.133	.151	.155	.155
f_{h_2}/f_t	.567	.550	.565	.619	.556	.581
f_{h_3}/f_t	1.26	1.25	1.29	1.40	1.35	1.37

(d) Configuration IV

Model 9 left panel $\bar{m}$ = 0.00211 slug

η	m, slugs/ft	r_a^2	a	x_a	b/b_r
0.379	0.00453	0.242	-0.276	0.180	0.7163
.462	.00394	.235	-.252	.160	.6493
.544	.00448	.274	-.224	-.084	.[illegible]
.628	.00398	.330	-.200	-.142	.[illegible]
.707	.00379	.298	-.162	-.236	.[illegible]
.792	.00165	.257	-.122	.044	.[illegible]
.877	.00123	.271	-.060	.020	.[illegible]
.940	.00934	.334	.022	-.034	.[illegible]

Measured natural frequencies

Item	Model 8		Model 9	
	Left	Right	Left	Right
f_{h_1}	84.2	82	81.5	83.3
f_{h_2}	293	283	267	277
f_{h_3}	687	692	640	657
f_t	482	452	467	468
f_{h_1}/f_t	.175	.181	.175	.178
f_{h_2}/f_t	.608	.638	.572	.592
f_{h_3}/f_t	1.43	1.31	1.37	1.40

TABLE III.- COMPILATION OF EXPERIMENTAL RESULTS

(a) Ballast configuration I

Model	Run	Point	Wing-panel behavior[1]		M_e	ρ_e, slugs/cu ft	$\bar{\mu}_e$	V_e, ft/sec	f_e, cps		f_t, cps		f_e/f_t		$\frac{V_e}{b_s \omega_t \sqrt{\bar{\mu}_e}}$		q_e, lb/sq in.
			Left	Right					Left	Right	Left	Right	Left	Right	Left	Right	
1	1	1	D	D	0.796	0.00208	37.44	841.4	---	---	432	424	------	------	0.2560	0.2608	5.11
		2	F_1	F_1	.854	.00206	37.81	894.7	164	164			0.3796	0.3868	.2709	.2760	5.75
		3	E_1	E_1	.975	.00195	39.94	1002.9	175	175			.4051	.4127	.2954	.3010	6.80
	2	1	F_1	F_1	.808	.00207	37.63	855.3	166	166			.3842	.3915	.2596	.2645	5.27
		2	E_1	E_1	.975	.00194	40.15	1004.7	175	175			.4051	.4127	.2952	.3007	6.80
	3	1	F_1	F_1	.825	.00224	34.77	867.7	170	170			.3935	.4009	.2739	.2791	5.86
		2	E_1	E_1	.976	.00215	36.23	1002.8	178	178			.4120	.4198	.3101	.3160	7.50
		3	M	M	1.285	.00504	15.45	1177.1	---	---			------	------	.5575	.5680	24.27
	4	1	F_1	F_1	.829	.00232	33.57	882.7	169	169			.3912	.3986	.2836	.2890	6.29
		2	E_1	E_1	.986	.00229	34.01	1025.0	182	182			.4213	.4292	.3372	.3334	8.36
		3	M	M	1.255	.00582	13.38	1182.1	---	---			------	------	.6016	.6130	28.30
2	5	1	F_1	F_1	.664	.00390	19.97	709.2	208	208	427	431	.4871	.4826	.2989	.2961	6.83
	6	1	F_1	F_1	.745	.00252	30.91	799.9	188	188			.4403	.4362	.2710	.2685	5.61
	7	1	F_1	F_1	.813	.00211	36.91	869.8	160	163	431	431	.3712	.3782	.2641	.2641	5.41
		2	E_1	E_1	.986	.00194	40.15	1018.0	170	177			.3944	.4107	.2998	.2998	7.00
		3	M	M	1.302	.00442	17.62	1219.3	---	---			------	------	.5420	.5420	22.85
	8	1	F_1	F_1	.789	.00258	30.19	840.9	172	175			.3991	.4060	.2856	.2856	6.35
		2	X	E_1	1.041	.00287	27.14	1066.6	---	209			------	.4849	------	.3820	11.35

[1]Wing-panel behavior code:

F - flutter
E - end of flutter
N - no flutter
D - low damping conditions
M - maximum dynamic pressure - no flutter
X - no data obtained

Subscripts:

1 - associated with first occurrence of flutter
2 - associated with second occurrence of flutter

TABLE III.- COMPILATION OF EXPERIMENTAL RESULTS - Continued

(c) Ballast configuration II

Model	Run	Point	Wing-panel behavior[1]		M_e	ρ_e, slugs/cu ft	E_e	V_e, ft/sec	f_e, cps		f_t, cps		f_e/f_t		$\frac{V_e}{f_e b_{1/4 \text{ tip}}}$		q_e, lb/sq in.
			Left	Right					Left	Right	Left	Right	Left	Right	Left	Right	
4	9	1	F_1	N	1.009	0.00201	37.56	939.9	194	---	457	474	0.424	-----	0.2619	------	6.15
		2	F_2		1.068	.00191	41.06	1020.6	194	---			.424	-----	.2773	------	6.90
	10	1	N	F_1	.661	.00237	38.71	898.4	---	167			-----	0.352	------	0.2490	5.91
		2	F_1		.958	.00202	39.69	941.1	193				.428		.2629		6.22
		3	E_1	E_1	.968	.00158	40.49	931.7	193	170			.428	.359	.2643	.2644	6.16
		4	M	M	1.339	.00490	18.56	1202.3	---	---			-----	-----	.5231	.5043	24.61
	11	1	N	F_1	.89	.00204	39.29	939.8	---	167			-----	.352	------	.2553	6.21
		2	F_1		.943	.00199	40.28	976.8	191				.418		.2700		6.60
		3	E_1	E_1	1.031	.00191	41.36	1053.0	191	170			.418	.363	.2861	.2758	7.48
		4	M	M	1.319	.00614	13.09	1201.9	---	---			-----	-----	.5959	.5645	30.82
	12	1	D_1	N	.723	.00338	23.71	751.6	---	---			-----	-----	.2716	------	6.64
		2	F_1		.785	.00344	23.30	763.1	213	---			.460	-----	.2782	------	6.96
	13	1	D_1	N	.652	.00417	19.22	692.0	---	---			-----	-----	.2774	------	6.96
		2	F_1		.666	.00431	18.34	701.3	221	---			.484	-----	.2842	------	7.47
	14	1	N	F_1	.873	.00220	36.43	908.0	---	163			-----	.344	------	.2552	6.32
		2	F_1		.907	.00217	36.94	937.6	200				.438		.2715		6.69
		3		E_1	.938	.00217	36.94	964.5		179				.369		.2692	7.03
		4	E_1		.988	.00215	37.28	1008.4	200	---			.438	-----	.2906	------	7.62
		5	M	M	1.300	.00615	13.03	1197.8	---	---			-----	-----	.5836	.5626	30.62
	15	1	F_1	N	.793	.00251	31.93	839.9	200	---			.438	-----	.2616	------	6.17
		2		F_1	.833	.00248	31.81	876.7		173				.365		.2637	6.74
		3		E_1	.983	.00260	30.93	1003.6		204				.430		.3082	9.20
		4	E_1		1.020	.00264	30.36	1040.0	216	---				-----	.3322	------	9.91
		5	M	M	1.146	.00705	11.37	1090.1	---	---			-----	-----	.5689	.5485	29.12
	16	1	F_1	N	.785	.00260	30.83	833.4	196	---			.429	-----	.2641	------	6.29
		2		F_1	.863	.00266	30.13	904.7		160				.380		.2796	7.58
		3		E_1	.975	.00280	28.62	1003.2		200				.422		.3182	9.77
		4	E_1		1.003	.00281	28.52	1021.9	217	---			.475	-----	.3382	------	10.35
		5	F_2	N	1.092	.00434	18.47	1087.8	470	---			1.028	-----	.454	------	17.83

[1]Wing-panel behavior code:

F - flutter
E - end of flutter
N - no flutter
D - low damping conditions
M - maximum dynamic pressure - no flutter
X - no data obtained

Subscripts:

1 - associated with first occurrence of flutter
2 - associated with second occurrence of flutter

TABLE III.- COMPILATION OF EXPERIMENTAL RESULTS - Concluded

(c) Ballast configuration III

Model	Run	Point	Wing-panel behavior[1]		M_e	ρ_e, slugs/cu ft	$\bar{\mu}_e$	V_e, ft/sec	f_e, cps		f_t, cps		f_e/f_t		$\frac{V_e}{b_{eq}\sqrt{\bar{\mu}_e}}$		q_e, lb/sq in.
			Left	Right					Left	Right	Left	Right	Left	Right	Left	Right	

(d) Ballast configuration IV

Model	Run	Point	Wing-panel behavior[1]		M_e	ρ_e, slugs/cu ft	$\bar{\mu}_e$	V_e, ft/sec	f_e, cps		f_t, cps		f_e/f_t		$\frac{V_e}{b_{eq}\sqrt{\bar{\mu}_e}}$		q_e, lb/sq in.
			Left	Right					Left	Right	Left	Right	Left	Right	Left	Right	

[1]Wing-panel behavior code:

F - flutter
E - end of flutter
N - no flutter
D - low damping conditions
M - maximum dynamic pressure - no flutter
X - no data obtained

Subscripts:

1 - associated with first occurrence of flutter
2 - associated with second occurrence of flutter

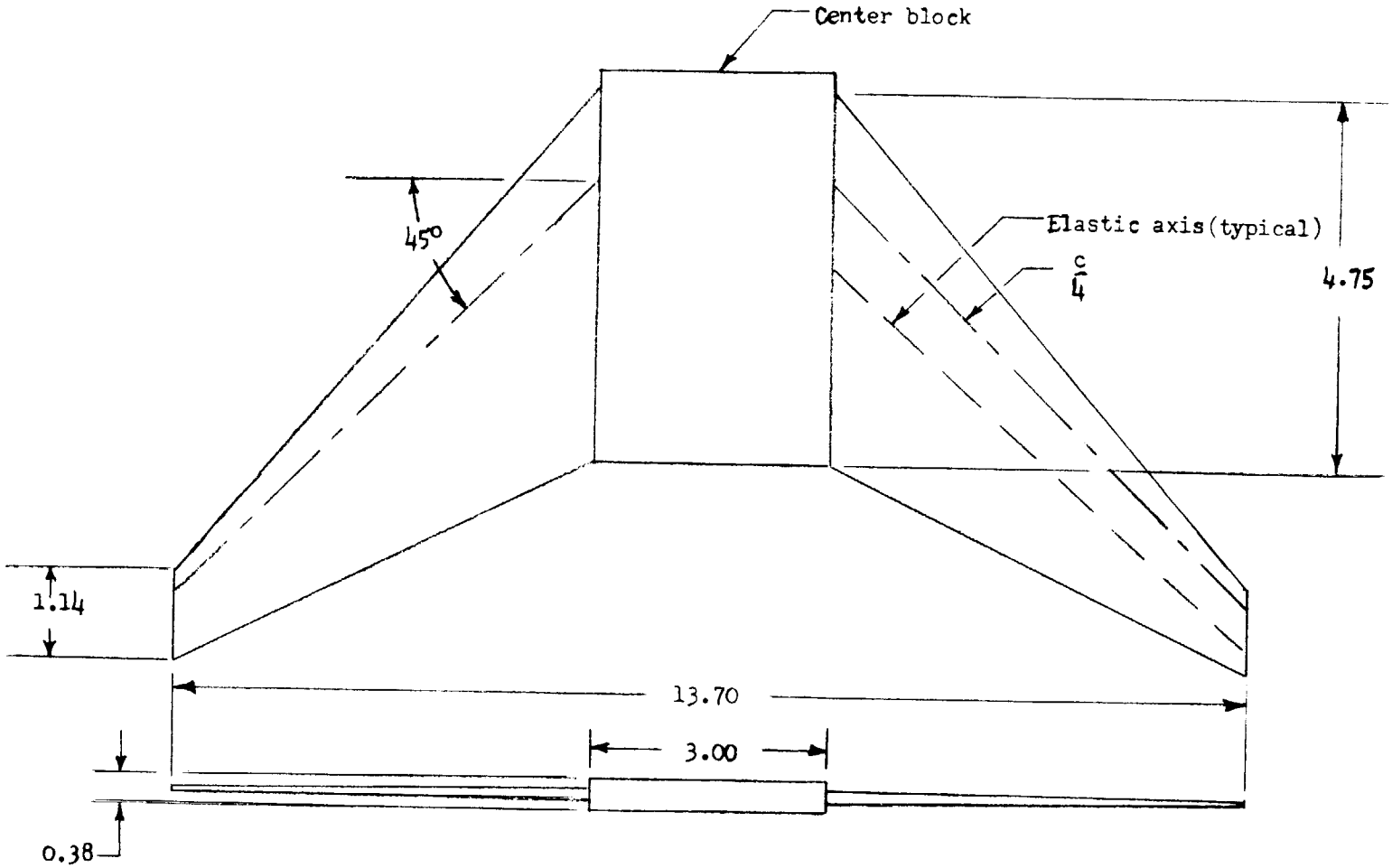

(a) Model dimensions.

Figure 1.- Drawings of flutter models showing dimensions, ballast locations, node lines, and associated natural frequencies. All dimensions in inches.

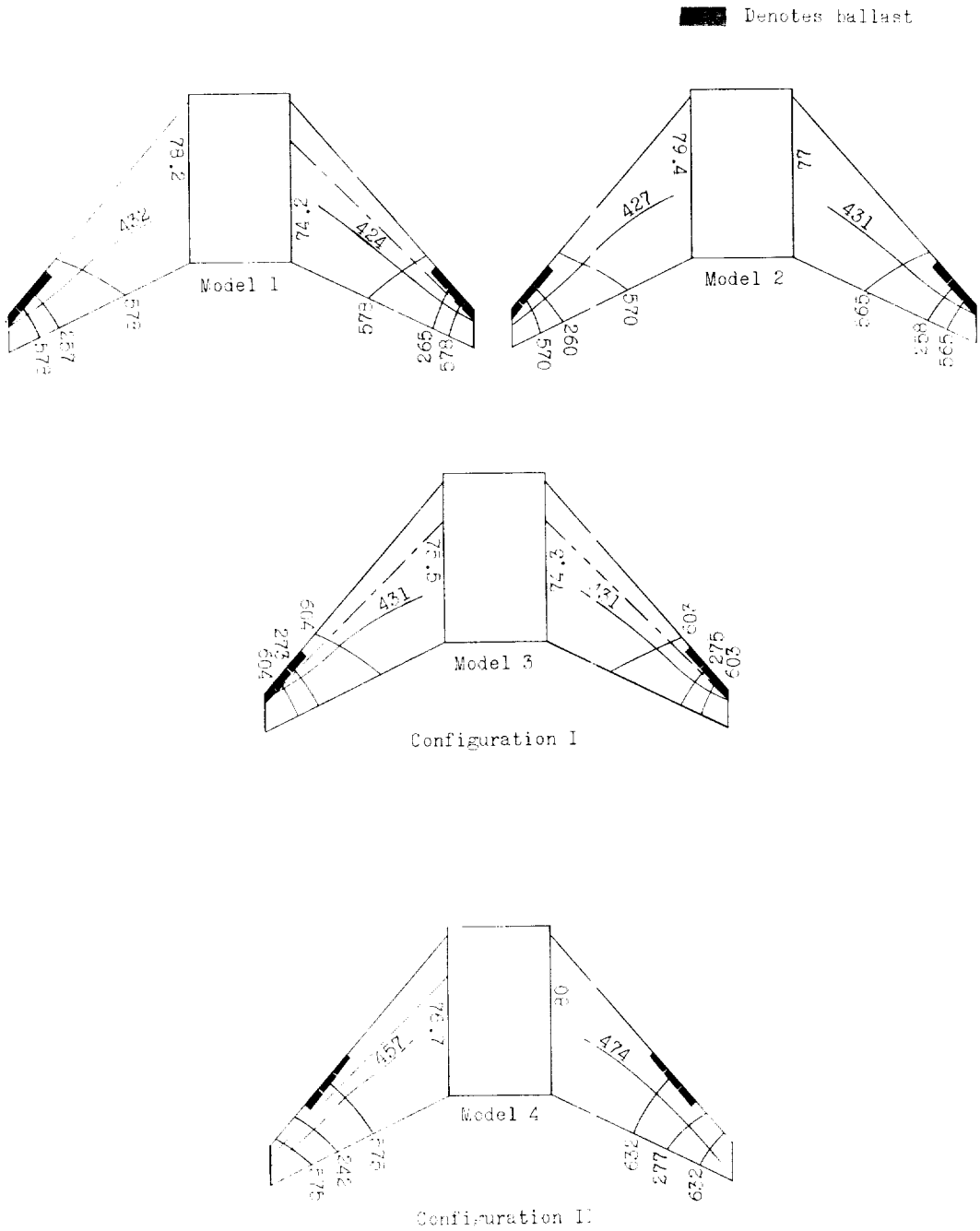

(b) Configurations I and II.

Figure 1.- Continued.

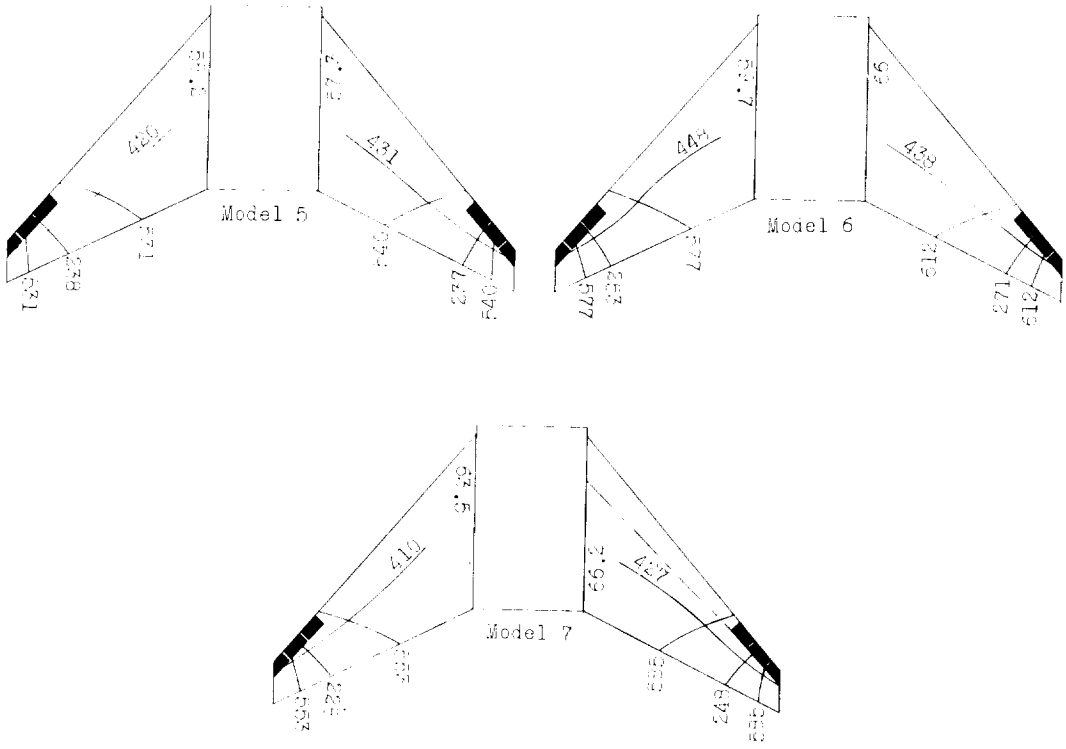

Configuration III

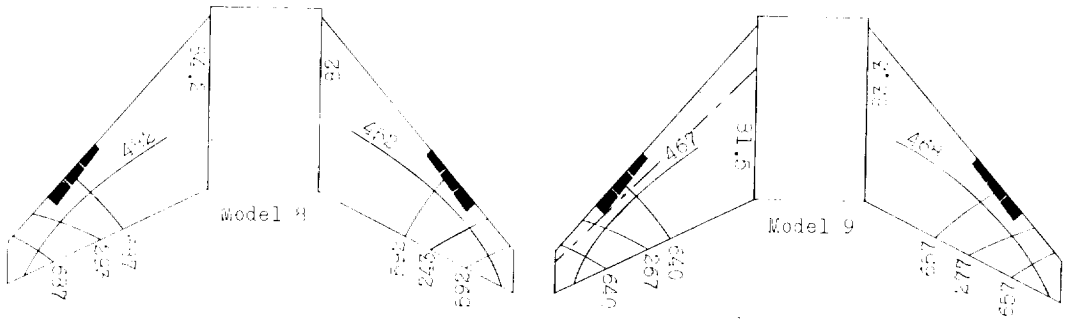

Configuration IV

(c) Configurations III and IV.

Figure 1.- Concluded.

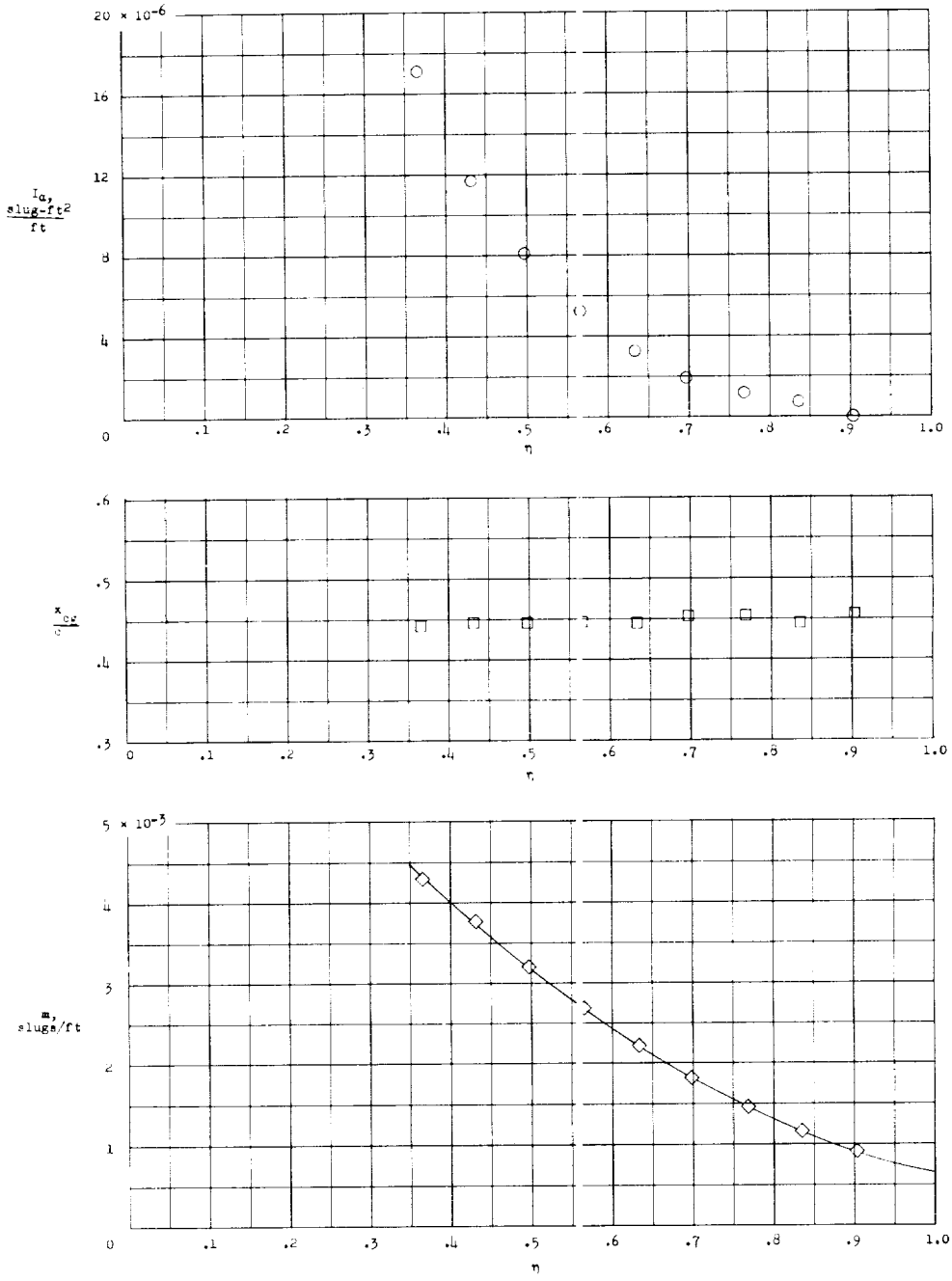

(a) Basic wing data.

Figure 2.- Spanwise variation of measured mass per unit length, center-of-gravity position, and mass moment of inertia per unit length for basic-wing and ballasted-wing configurations.

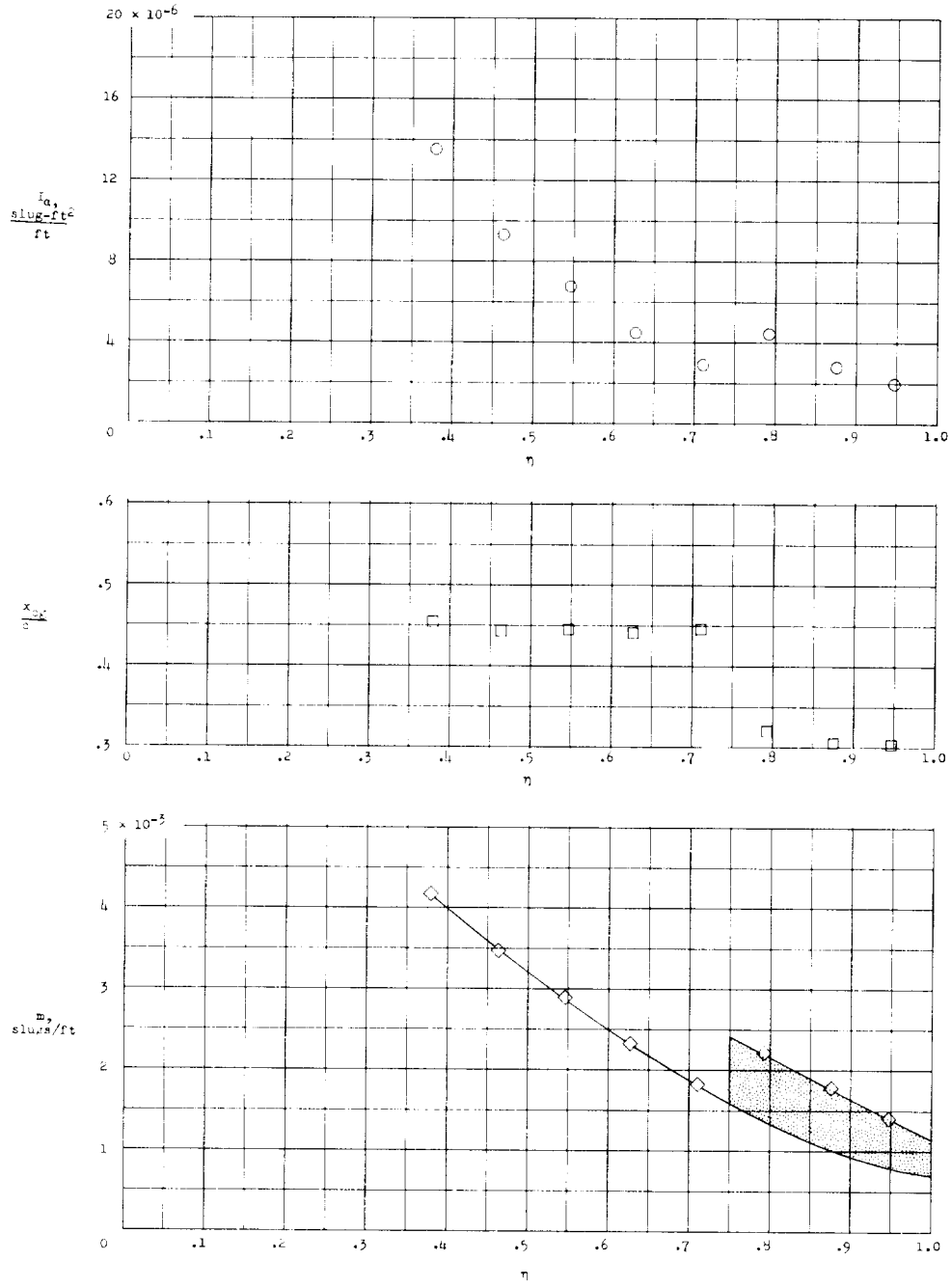

(b) Ballast configuration I (model 1, right panel).

Figure 2.- Continued.

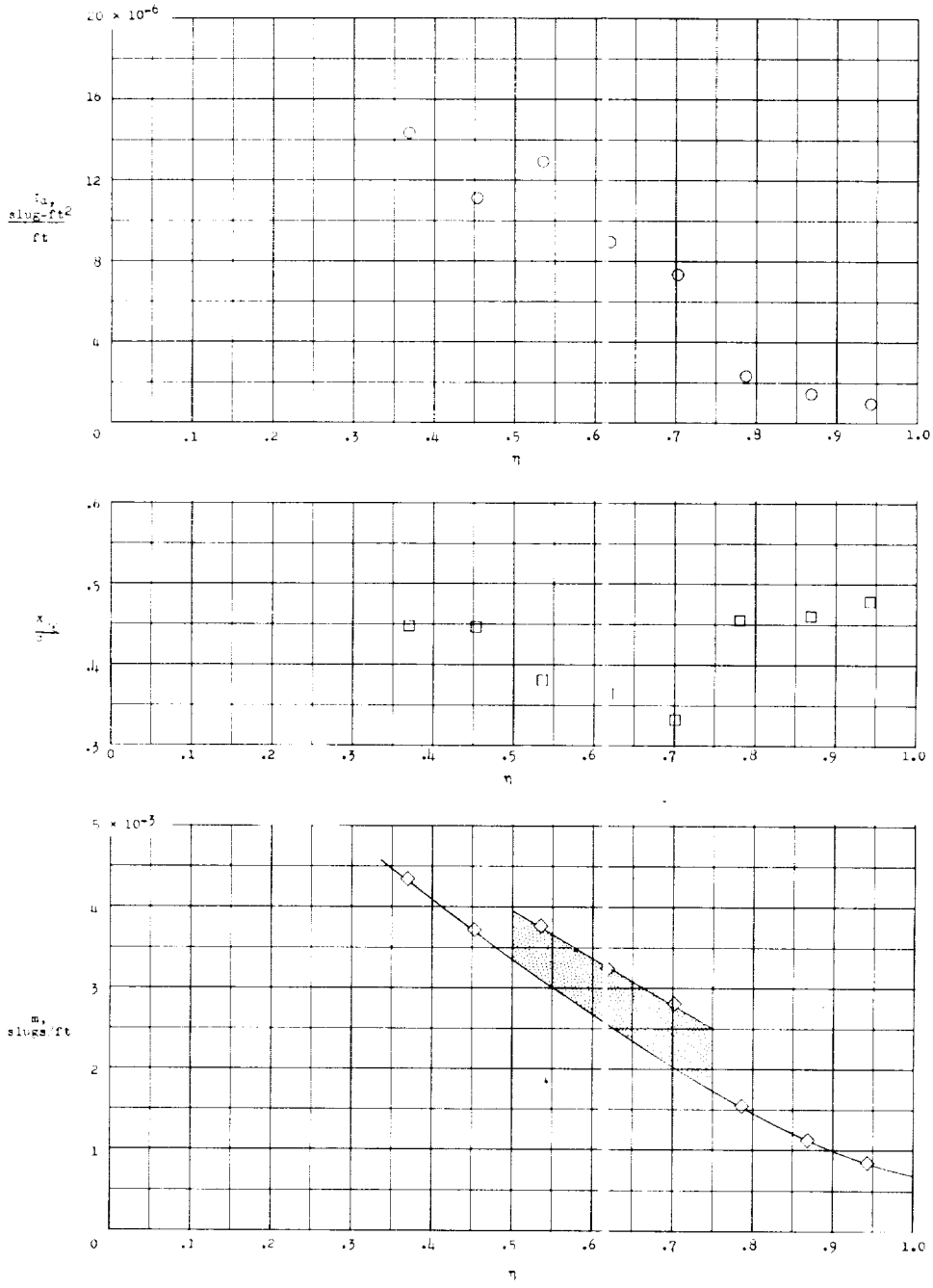

(c) Ballast configuration II (model 4, left panel).

Figure 2.- Continued.

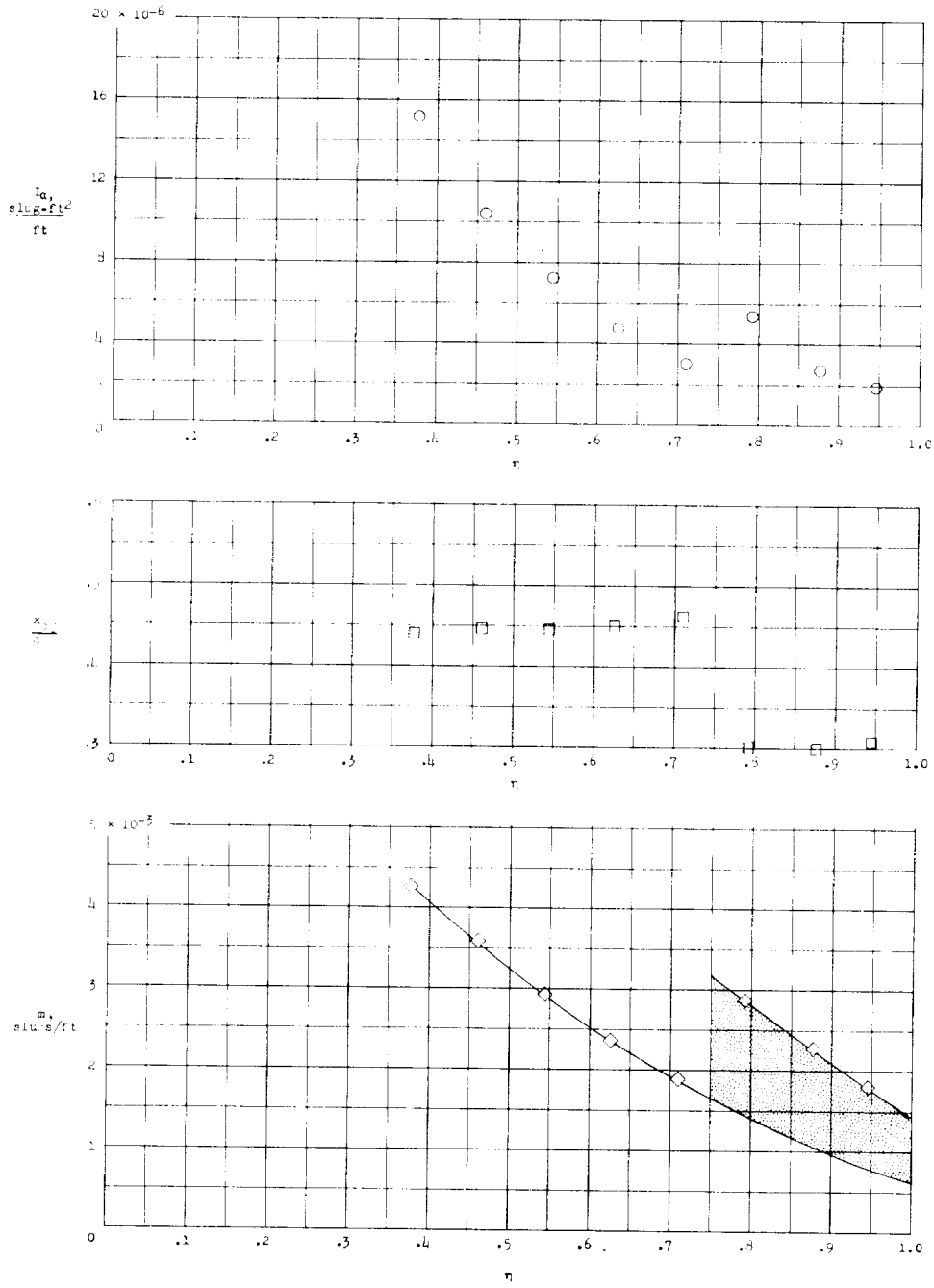

(d) Ballast configuration III (model 7, right panel).

Figure 2.- Continued.

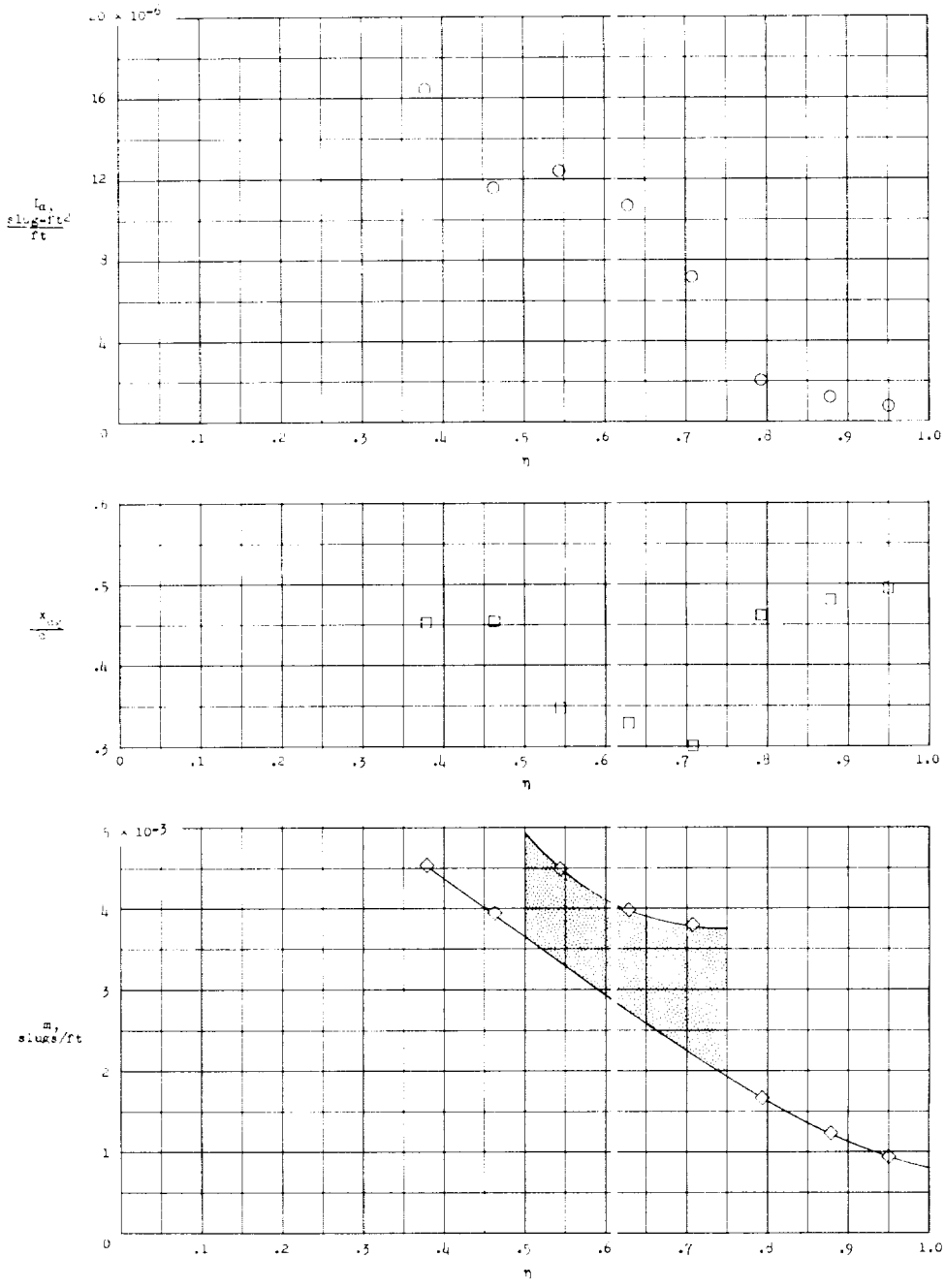

(e) Ballast configuration IV (model 9, left panel).

Figure 2.- Concluded.

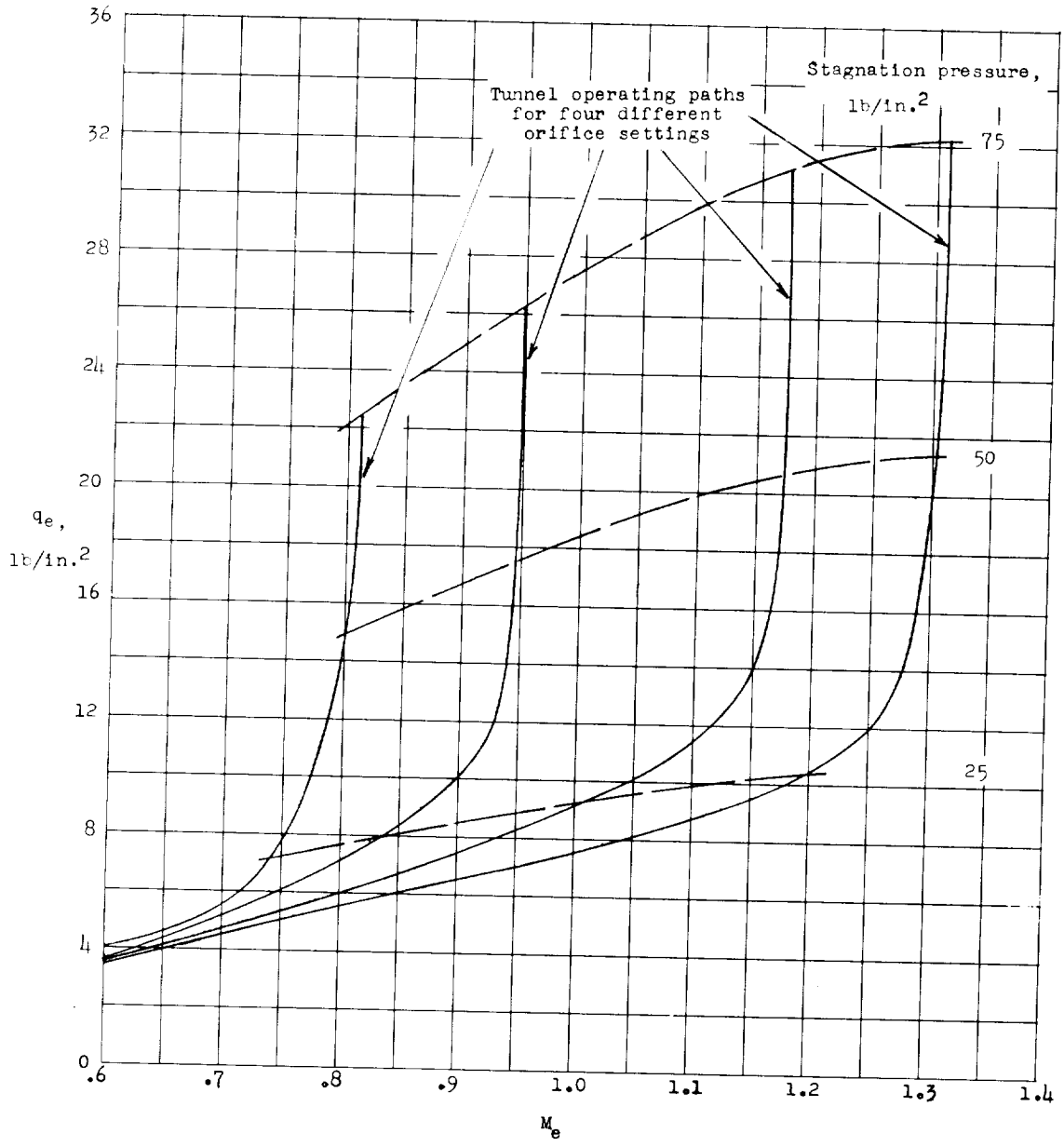

Figure 3.- Operating characteristics of the Langley transonic blowdown tunnel.

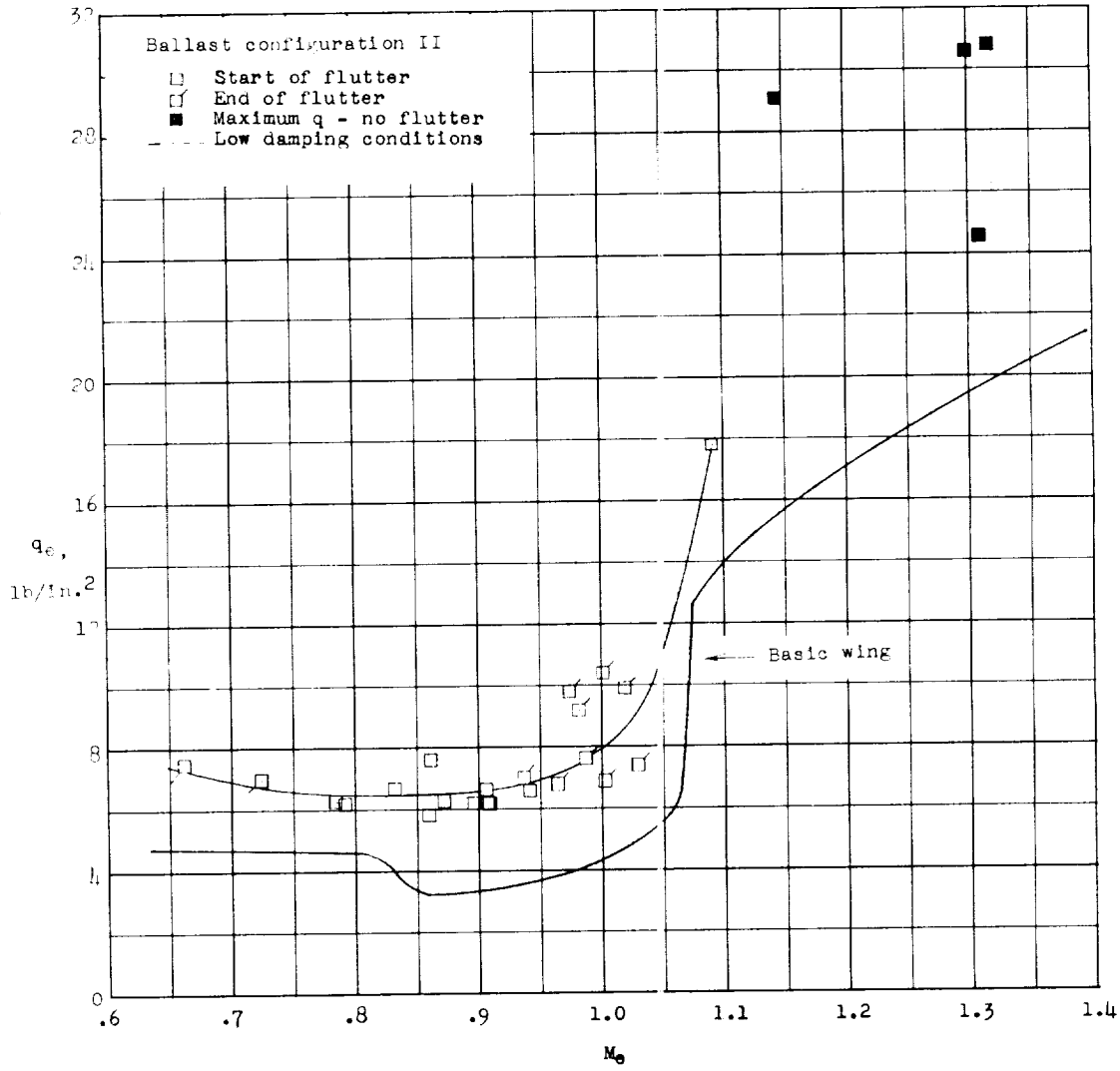

(b) Models of ballast corfiguration II.

Figure 5.- Continued.

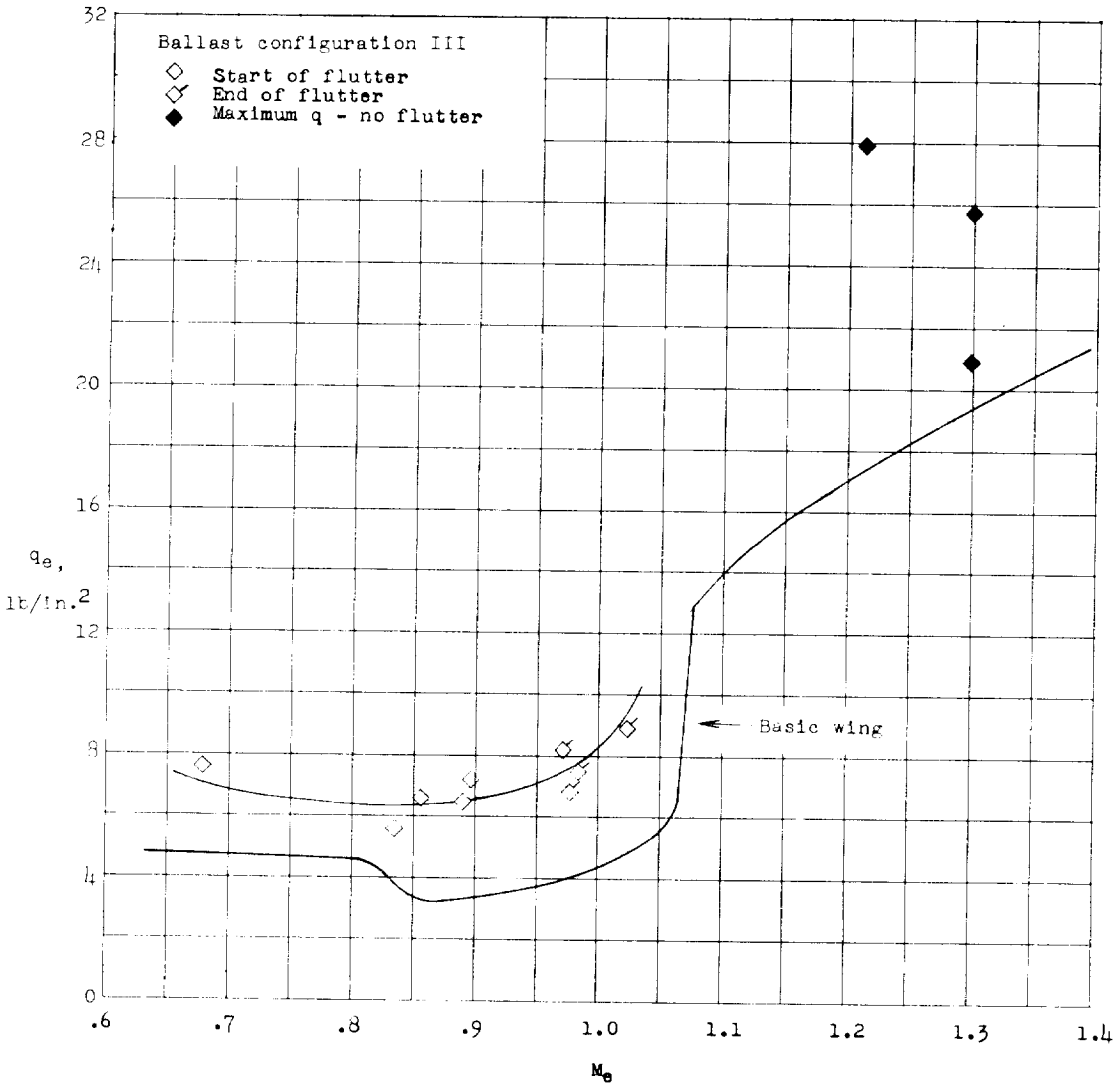

(c) Models of ballast configuration III.

Figure 5.- Continued.

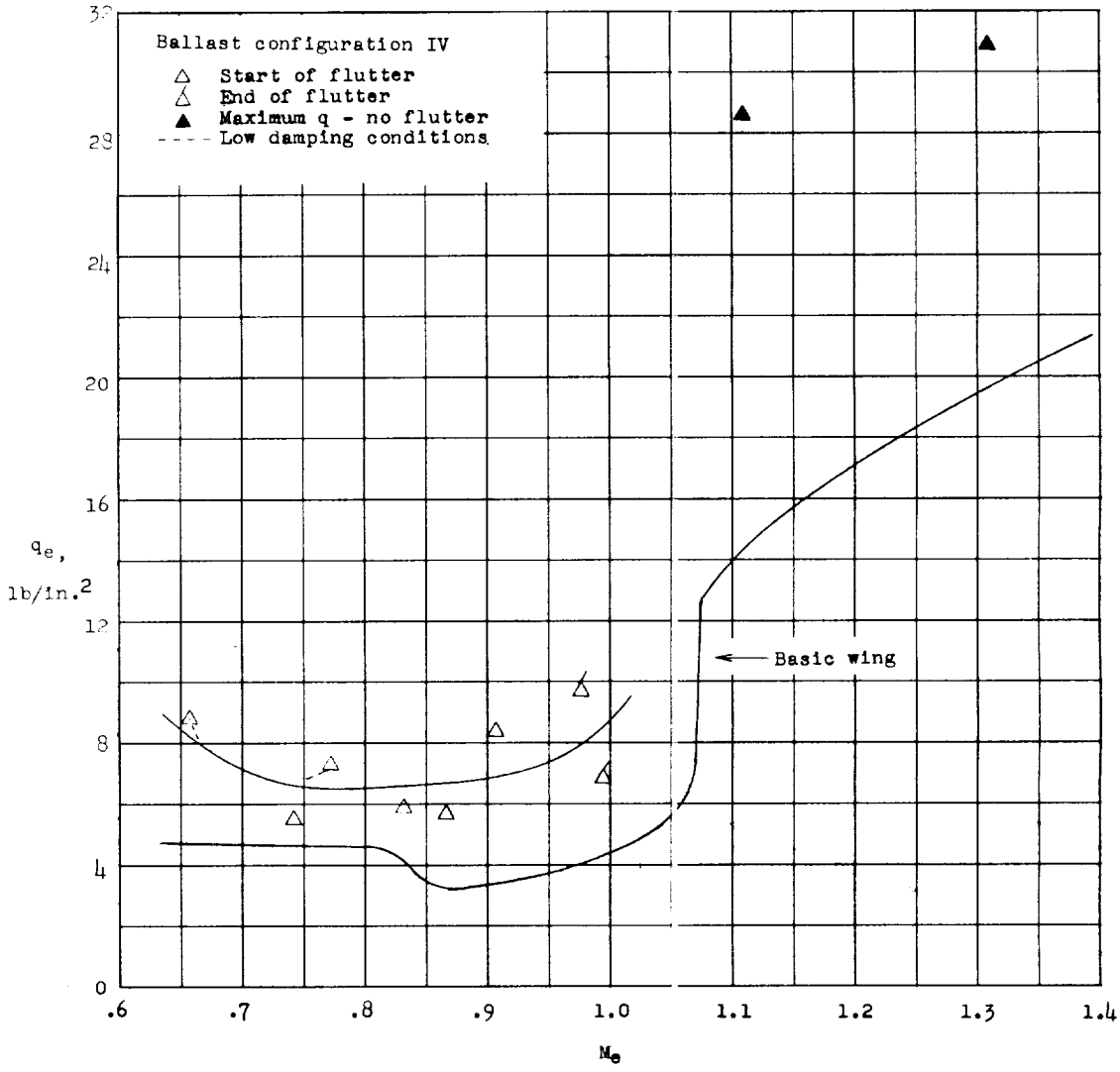

(d) Models of ballast configuration IV.

Figure 5.- Concluded.

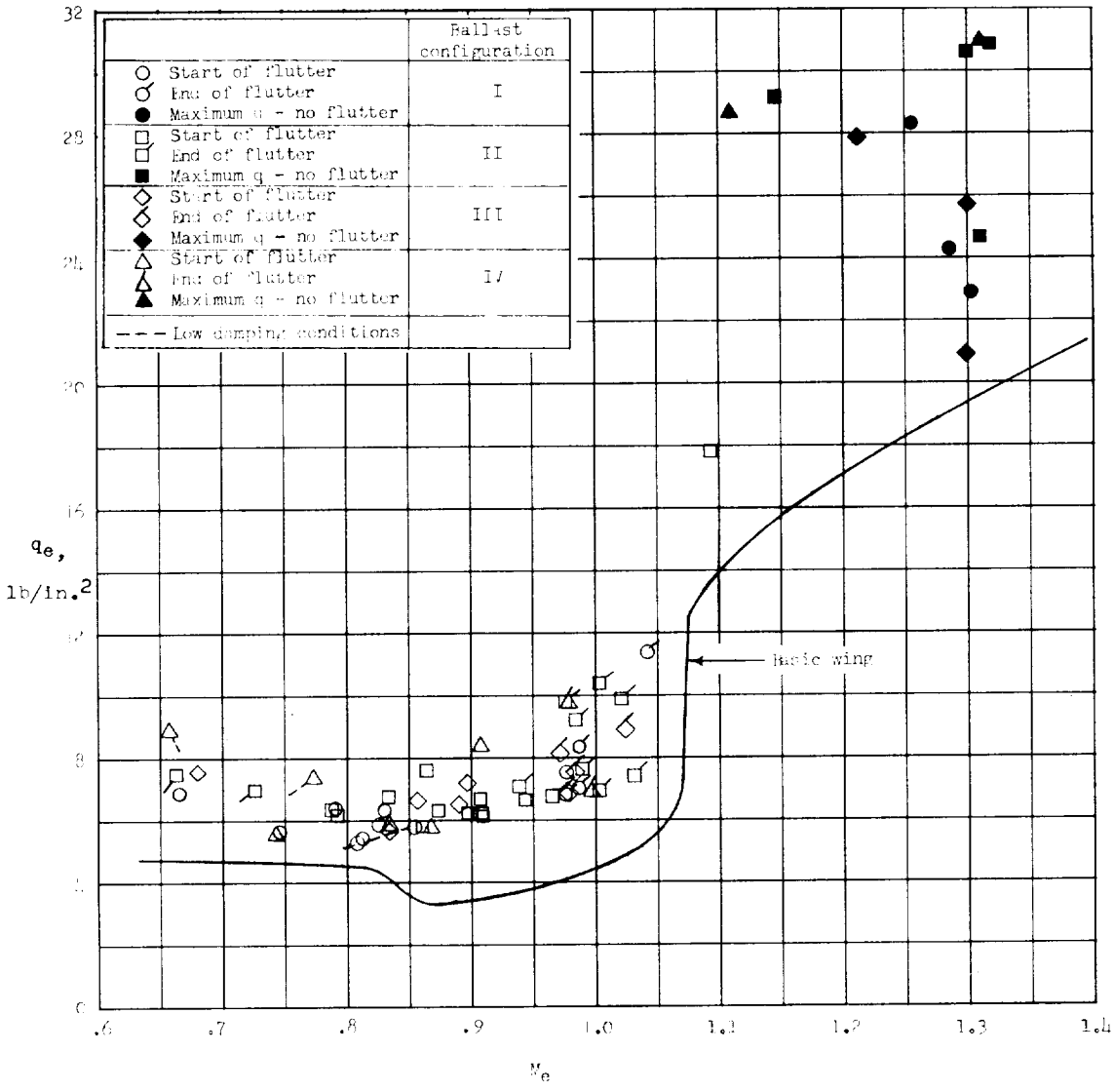

Figure 6.- Variation of dynamic pressure required for flutter with Mach number for ballast configurations I, II, III, and IV.

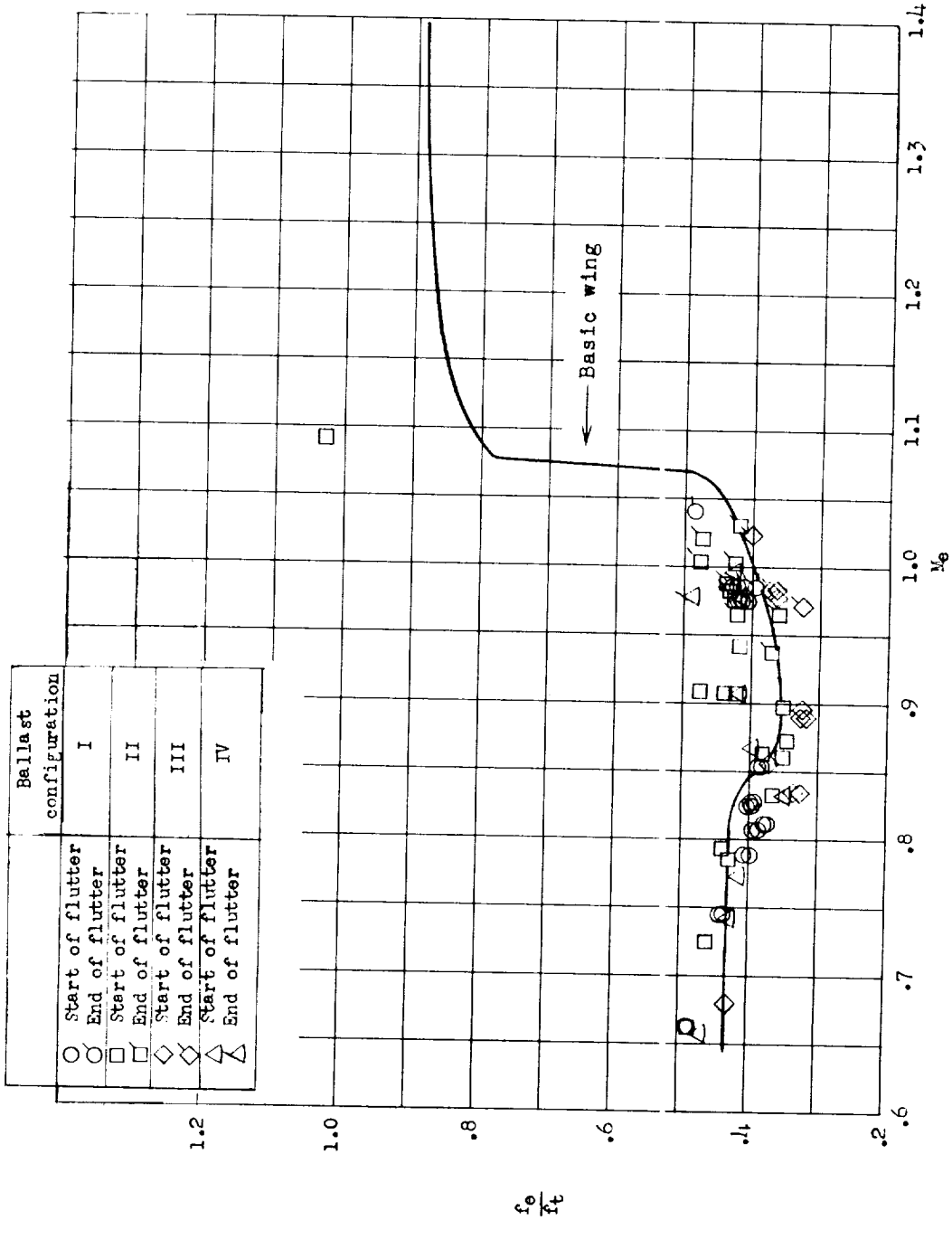

Figure 7.- Variation of the ratio of experimental flutter frequency to measured torsional frequency with Mach number for four ballast configurations.